

---

## Pulse distortion and optimum transmit waveform for pulse-based UWB communications

---

Chenming Zhou

Department of Electrical and Computer Engineering,  
Carnegie Mellon University,  
Pittsburgh, PA 15237, USA  
E-mail: czhou@cmu.edu

Robert C. Qiu\*

Department of Electrical and Computer Engineering,  
Tennessee Technological University,  
Cookeville, TN 38505, USA  
E-mail: rqi@tntech.edu  
\*Corresponding author

**Abstract:** This paper initiates a new investigation of optimum transmission waveforms in the presence of per-path pulse wave shape distortion – a physical mechanism unique to impulsive signals. First, the transient electromagnetic analysis is carried out to derive, for the first time, closed-form expressions for the impulse responses of several canonical channels that are suitable for communication engineers. Second, numerical calculation using the inverse Fourier transform of the frequency-domain expressions is compared with the derived closed-form expressions, to verify the validity of these derived impulse responses. Third, propagation mechanisms responsible for multipath and per-path pulse shape distortion can be clearly identified using the closed-form impulse responses. Finally, using these closed-form expressions as a departure point, optimum transmission waveforms determined by a Fredholm integration equation are investigated, for different physical mechanisms, including one path or no multipath (wedge), two paths (rectangular building) and more than two paths (two half plane waveguide).

**Keywords:** optimum waveform design; UWB; time domain UTD/GTD; ray tracing; deterministic channel modelling; pulse distortion; time reversal.

**Reference** to this paper should be made as follows: Zhou, C. and Qiu, R.C. (2009) 'Pulse distortion and optimum transmit waveform for pulse-based UWB communications', *Int. J. Ultra Wideband Communications and Systems*, Vol. 1, No. 1, pp.32–48.

**Biographical notes:** Chenming Zhou is a Research Scientist at the Department of Electrical and Computer Engineering at Carnegie Mellon University, Pittsburgh, USA. He completed his PhD in Electrical Engineering from Tennessee Technological University in 2008. Since 2004 he has been researching in wireless communication and networking systems, in particular ultrawideband.

Robert Caiming Qiu (IEEE S'93-M'96-SM'01) received his PhD in EE from Polytechnic Institute of New York University. He is a Professor in the Department of ECE, Tennessee Technological University, Cookeville, TN. He was Founder-CEO of Wiscom Technologies, Inc., for WCDMA chipsets. Wiscom was sold to Intel. He worked for GTE Labs (now Verizon), Waltham, MA and Bell Labs, Lucent, Whippany, NJ. He holds over five patents in WCDMA and authored over 50 journal papers/book chapters. He serves as an Associate Editor of *IEEE Transactions on Vehicular Technology*. He is a Guest Book Editor on UWB from John Wiley and three special issues.

---

### 1 Introduction

Ultra-wideband impulsive radio transmission requires a paradigm shift in thinking (Scholtz, 1993; Win and Scholtz, 2000; Roy et al., 2004; Qiu et al., 2005a, 2005b; Shen et al. 2006), especially for modulation waveform using short impulsive pulses. During transmission, these impulsive

pulses will interact with the propagation environment (Qiu, 2006c) – a process involves transient analysis of electromagnetic wave propagation. Although the physical mechanisms are well investigated through previous work, e.g., Qiu (2002), Qiu (2004), Qiu (2006a) and Qiu et al. (2005c), the impacts of these mechanisms on system design

(Qiu, 2005; Qiu et al., 2006a; Zhou and Qiu, 2007) require more attention.

The dispersive channel causes two pulse distortion mechanisms to the incident impulsive signal:

- 1 multipath
- 2 per-path wave shape distortion.

The first mechanism is common to narrowband systems and UWB impulse radios. The second mechanism that is included in IEEE 802.15.4a channel model (Molisch, 2004) is unique to impulse radio (Qiu, 2006c) – first investigated in Qiu (1996) and Qiu and Lu (1999). This mechanism is caused by the frequency-dependent physical processes, such as diffraction and media absorption. Time reversal (Qiu et al., 2006b; Zhou and Qiu, 2006a; Qiu, 2006b; Qiu et al., 2007c; Qiu et al., 2006c; Zhou et al., 2007b; Guo et al., 2007a; Qiu et al., 2007b; Calderon and Qiu, 2007; Qiu et al., 2007a; Zhou et al., 2007a) is an effective approach suggested to compensate for this unique mechanism, to simplify the transceiver of the generalised RAKE in Qiu et al. (2006a). This paper is different from previous work in that the optimum modulation waveforms are investigated in the presence of per-path wave shape distortion. In the absence of multipath and per-path wave shape distortion, any pulse waveform performs the same. In the presence of per-path wave shape distortion, the optimisation of pulse waveform is required, even in the absence of multipath – unique to UWB impulsive signal.

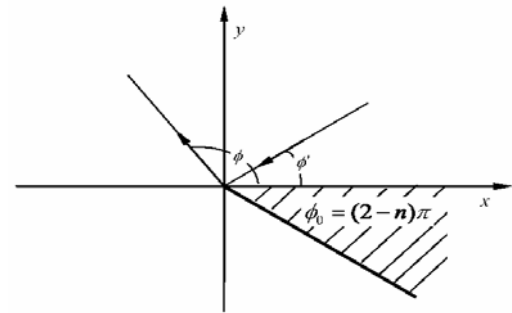
The objective of this paper is to model several canonical channels using a transient electromagnetic analysis and to derive the optimum modulation waveforms for impulsive pulses. The contributions of this paper are as follows. First, the time domain impulse responses for several diffraction environments have been derived for the first time. Specifically, the closed-form impulse responses for perfect electromagnetic conducting wedge, large rectangular plates and parallel planes waveguide, are derived. The received signal is calculated, through convolution, using these time domain impulse responses. The impulsive pulse waveforms passing through these channels are compared with their original waveforms. The comparison shows that these pulses could be distorted by diffraction mechanisms. Secondly, the results, numerically calculated from frequency domain by applying an inverse fast Fourier Transform (IFFT), are in close agreement with the derived closed-form time domain results. Third, given the time domain channel impulse responses (CIRs), the optimum transmission waveforms, in the sense of maximising the signal to noise ratio (SNR) at the receiver, are obtained – under the constraint of fixed transmitted power.

## 2 Pulse distortion and its impact on UWB system design

### 2.1 Per-path pulse shape distortion caused by wide bandwidth

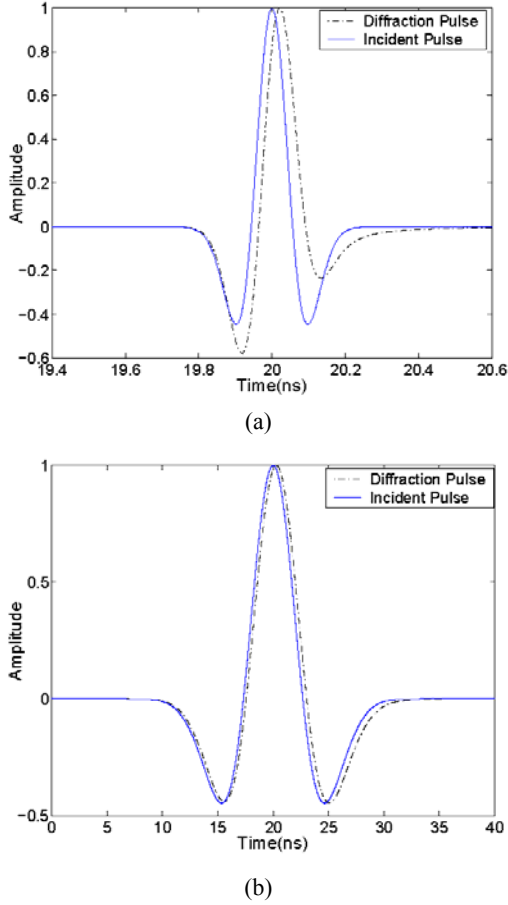
The traditional (narrowband) communication theory is based on the assumption of no per-path wave shape distortion, which suggests that the received signal consists of a train of the replicas of the transmitted pulse. This assumption is valid when the signal bandwidth is not wide. For ultra-wideband signals, this assumption is invalid. As a quick example, Figure 2 shows the wave shape distortions for two pulses with different bandwidths after they pass through a wedge channel – the transmitted pulse is diffracted by a perfectly electrically conducting (PEC) wedge shown in Figure 1.

**Figure 1** Plane wave is normally incident on a perfectly conducting wedge



The incident pulse in Figure 2(a) is a second order derivative of Gaussian waveform with a pulse width of 0.2 ns, corresponding a 5.86 GHz 10-dB bandwidth in the frequency domain and the pulse in Figure 2(b) is about 10 ns wide, corresponding a 128 MHz 10-dB bandwidth. For the convenience of waveform comparison, the amplitudes of both incident waveform and the diffracted waveform have been normalised. It is evident that the shorter pulse (wider bandwidth) experiences more distortion than the longer pulse after they pass through the same diffraction channel. When the signal bandwidth is not very wide [e.g., the 128 MHz waveform in Figure 2(b)], the distortion caused by channel is negligible. However, when the signal bandwidth is increasing, the distortion becomes noticeable. The details of the calculation of the diffracted waveform for a wedge channel will be given in Section 5.1. Since the distortion illustrated in Figure 2 is independent of multipath, we call this physical phenomenon the per-path wave shape distortion. It will be clear in the derived closed-form impulse response later that only one path is present in this configuration.

**Figure 2** Pulse distortion for pulses with different bandwidths (a) short pulse diffraction (b) wide pulse diffraction (see online version for colours)



Notes: The incident pulse for (a) is about 0.2 ns wide, corresponding to a 10 dB bandwidth of 5.86 GHz and for (b) is about 10.2 ns wide, corresponding to a 10 dB bandwidth of 128 MHz. The amplitudes of incident pulse and diffracted pulse were scaled to the same level to better compare the waveforms.

## 2.2 The impact of pulse distortion on system design

Consider a communication system illustrated in Figure 3. Here,  $p(t)$  is the transmitted pulse waveform and  $h(t)$  denotes the CIR. The received signal before  $c_1(t)$  can be written as

$$r(t) = p(t) * h(t) + n(t) = y(t) + n(t), \quad (1)$$

where  $n(t)$  is additive white Gaussian noise (AWGN) with a two-sided power spectral density of  $N_0/2$ . Given  $y(t) = p(t) * h(t)$ , a matched filter – matched to  $y(t)$  – provides the maximum signal-to-noise power ratio (SNR) at its output. The matched filter here can be virtually decomposed into two filters, with the first filter matched to the CIR  $h(t)$  and the second matched to the pulse waveform  $p(t)$ . As shown in Figure 3, this decomposition can be done

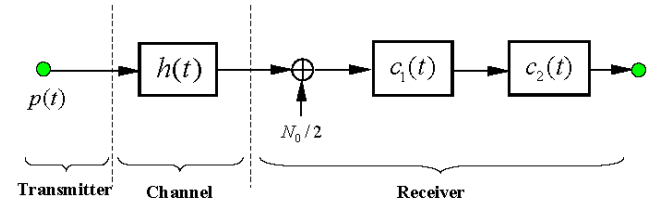
by setting  $c_1(t) = h(-t)$  and  $c_2(t) = p(-t)$ . A conventional channel is modelled as a tapped delay line, that is

$$h(t) = \sum_{l=1}^L \alpha_l \delta(t - \tau_l) \quad (2)$$

where  $L$  is the number of multipath components and  $\alpha_l$  and  $\tau_l$  are their individual amplitudes and delays. The received signals are just a train of replicas of the transmitted pulse, with different attenuations and time delays.

In practice, the estimation of  $h(t)$  is generally a very difficult task, especially when there is per-path pulse distortion for the wide band signals. The receiver suffers significant performance loss (as big as 4 dB), if the system is designed without the necessary compensation for pulse shape distortion (Qiu et al., 2005c). Along with system performance loss, this per-path pulse shape distortion can cause timing and synchronisation error as well. It has been shown in Qiu et al. (2005c) that the timing error caused by distortion due to cylinder diffraction can be much larger than the Cramer-Rao lower bound, thus is another fundamental issue that should be considered in system design.

**Figure 3** General model for wireless data transmission (see online version for colours)



A new channel model that takes into account per-path pulse shape distortion is then proposed in Qiu (2006c, 2006d)

$$h(t) = \sum_{l=1}^L h_l(t) * \delta(t - \tau_l) \quad (3)$$

where per-path impulse response  $h_l(t)$  includes both attenuation and distortion of the pulse when it passes through the channel along that path.

Note that per-path impulse response information can only be provided by the time domain framework, which justifies our effort for the time domain transient electromagnetic analysis.

## 3 CIRs for several canonical channels

In this section we study several simple propagation models that are mathematically tractable. For these models, the analytical results can often be obtained through exploring the physical mechanism behind it. These analytical results provide us unique insight into the signal propagation in practical environments which are usually formed by these simple models. In this section, we are aimed at deriving closed-form time domain CIR for these models. We will

first start with its frequency domain model and then transform it to time domain via the inverse Laplace transform. The idea is simple, but the analytical work is involved.

### 3.1 Wedge channel (one path)

Rather than seeking the exact solution for Maxwell's equations, the geometric theory of diffraction (GTD) uses generalisation of Fermat's principle to find high-frequency harmonic Maxwell equation solutions for many complicated objects. The uniform theory of diffraction (UTD) was proposed to complement GTD in the situations where GTD was invalid (Kouyoumjian and Pathak, 1974). The original GTD/UTD was proposed in frequency domain and then was widely used in narrowband radio propagation, e.g., for path loss prediction. In 1990, time domain UTD was firstly derived by Veruttipong in 1990 by applying an inverse Laplace transform to the corresponding frequency domain results. The TD-UTD diffraction coefficient for a straight PEC wedge illustrated in Figure 1 can be expressed as (Veruttipong, 1990)

$$D^{s,h}(t) = \frac{-1}{2n\sqrt{2\pi}\sin\beta_0} \sum_{m=1}^4 K_m^{s,h} F(X_m, t) \quad (4)$$

where

$$\begin{aligned} K_1^{s,h} &= \cot\left(\frac{\pi + \phi - \phi'}{2n}\right) \\ K_2^{s,h} &= \cot\left(\frac{\pi - \phi - \phi'}{2n}\right) \\ K_3^{s,h} &= \pm \cot\left(\frac{\pi + \phi + \phi'}{2n}\right) \\ K_4^{s,h} &= \pm \cot\left(\frac{\pi - \phi + \phi'}{2n}\right) \end{aligned} \quad (5)$$

and

$$F(X_m, t) = \frac{X_m}{\sqrt{\pi ct} \left(t + \frac{X_m}{c}\right)} u(t) \quad (6)$$

where the unit step function  $u(t)$  is defined as

$$u(t) = \begin{cases} 1, & t \geq 0 \\ 0, & t < 0. \end{cases}$$

The value of  $X_m$  in (6) is given by

$$\begin{aligned} X_1 &= 2L \cos^2 \left( \frac{2n\pi N^+ - (\phi - \phi')}{2} \right) \\ X_2 &= 2L \cos^2 \left( \frac{2n\pi N^- - (\phi - \phi')}{2} \right) \\ X_3 &= 2L \cos^2 \left( \frac{2n\pi N^+ - (\phi + \phi')}{2} \right) \\ X_4 &= 2L \cos^2 \left( \frac{2n\pi N^- - (\phi + \phi')}{2} \right) \end{aligned} \quad (7)$$

where  $N^\pm$  is the nearest integer solution of equation  $2n\pi N^\pm - \theta^\pm = \pm\pi$ , and  $L$  is the distance parameter determined by the incident wavefront. For plane wave incidence, we have  $L = r \sin^2 \beta_0$ , where  $r$  is the distance along the diffraction ray from the edge to the observation point. The rest of parameters used in (4)–(7) are described as follows:

- 's,h' soft and hard boundary conditions
- $n$  the parameter describing wedge angle; wedge angle  $\phi_0 = (2-n)\pi$
- $\beta_0$  the angle between the edge and the incident ray
- $\phi$  the angle between the wedge surface and the diffraction ray
- $\phi'$  the angle between the wedge surface and the incident ray.

These parameters are also illustrated in Figure 1, which shows a special case when  $\beta_0 = \pi/2$ .

If the observation angle is not in the transition zone, we have the time domain diffraction coefficient for GTD (Keller) solution (Veruttipong, 1990)

$$D^{s,h}(t) = \frac{1}{\sqrt{t}} u(t) \sqrt{\frac{c}{2}} \frac{\sin \frac{\pi}{n}}{n\pi \sin \beta_0} \cdot \left[ \frac{1}{\cos \frac{\pi}{n} - \cos \left( \frac{\phi - \phi'}{n} \right)} \mp \frac{1}{\cos \frac{\pi}{n} - \cos \left( \frac{\phi + \phi'}{n} \right)} \right] \quad (8)$$

Veruttipong's TD wedge diffraction coefficient given in (4) is a special case of the diffraction coefficient for curved wedge in Rousseau and Pathak (1995), where an analytical signal representation for the transient fields has been used. The details for analytical TD-UTD will be given in Section 5.1.2.

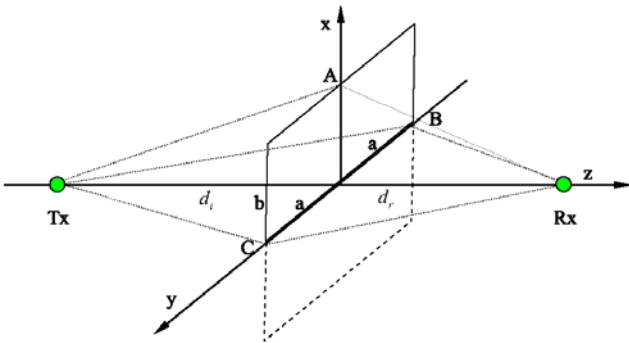
### 3.2 Rectangular building (two paths)

Rectangular PEC plate (building) illustrated in Figure 4 is one of the typical shapes often encountered in a practical propagation environment. Moreover, a lot of obstacles in the propagation environment can be approximated by a rectangular plate, with a limited degree of accuracy (Mokhtar and Lazaridis, 1999). This model has been widely studied in the past decades. However, most of the research is focused on frequency domain such as path loss prediction under different frequency bands. In the following, we will investigate its time domain characteristics such as pulse distortion introduced by diffraction of the edges of the building – this configuration has more than one edge compared with wedge in Figure 1. We will also analyse the optimum transmit waveform, given such a rectangular plate model, based on the derived closed-form time domain CIR.

As illustrated in Figure 4, we consider a simple UWB channel consisting of a transmitter, a receiver and a rectangular PEC building that blocks the light of sight (LOS) transmission. In Figure 4,  $d_t$ ,  $d_r$  denote the distance from the building to the transmitter (Tx) and the receiver (Rx), respectively. The size of the building is  $2a \times b$ . The lower half plane plotted by dash line denotes the image of the building relative to the ground and is considered as perfectly absorbing.

A good analysis of the path loss prediction in frequency domain can be found in Mokhtar and Lazaridis (1999) and the references therein. Two different approaches, Fresnel-Kirchhoff scalar approach and GTD approach tracing up to four propagation rays, are applied below to study the diffraction effects of rectangular building.

**Figure 4** UWB pulse diffracted by a rectangular building (see online version for colours)



Notes: Tx: transmitter antenna, Rx: receiver antenna.  
 $d_t / d_r$  denotes the distance between Tx/Rx and the building. The size of the building is  $2a \times b$ .  
 The lower half plane plotted by dash line denotes the image of the building relative to the ground.

#### 3.2.1 Propagation model based on Fresnel-Kirchhoff integral

The Fresnel-Kirchhoff integral is one of the traditional approaches used to calculate the propagation loss due to the

blocking of a rectangular building. We define the channel transfer function as the ratio of the strength of the received signal to the transmitted signal. Mathematically, the transfer function can be expressed as  $H(j\omega) = \frac{E_r(j\omega)}{E_0(j\omega)}$ . Then the

transfer function describes the rectangular diffraction can be expressed as (Mokhtar and Lazaridis, 1999):

$$H(j\omega) = \frac{1}{2} \left[ 1 - 2j \int_0^A \exp(-j\frac{\pi}{2}y^2) dy \int_0^B \exp(-j\frac{\pi}{2}x^2) dx \right] e^{-jkd} \quad (9)$$

where  $k$  is the wavenumber and  $d$  is the propagation distance. In our case we have  $d = d_t + d_r$ . In (9), variable  $A$  and  $B$  are the normalised half width and normalised height of the building, given by

$$A = a \sqrt{\frac{2(d_t + d_r)}{\lambda d_t d_r}} \quad B = b \sqrt{\frac{2(d_t + d_r)}{\lambda d_t d_r}} \quad (10)$$

where  $\lambda$  is the wavelength. The validity of (9) is based on the condition that the distances to and from the obstacle must be greater than its dimensions and the wavelength, i.e.,  $d_t, d_r \gg a, b, \lambda$ .

In the following, we will derive the time domain CIR based on (9). We firstly work on one of the integrals and express them to a form ready for inverse Laplace transform.

$$\begin{aligned} \int_0^A \exp(-j\frac{\pi}{2}y^2) dy &= \int_0^A \exp\left\{-\left(\sqrt{\frac{\pi j}{2}}y\right)^2\right\} dy \\ &= \sqrt{\frac{2}{\pi j}} \int_0^{A'} \exp(-z^2) dz \\ &= \frac{1}{2}(1-j)(1 - \text{erfc}(A')) \end{aligned} \quad (11)$$

where  $z = \sqrt{\pi j / 2} y$  and the complementary error function is defined as

$$\text{erfc}(x) = \frac{2}{\sqrt{\pi}} \int_x^\infty \exp(-t^2) dt,$$

and

$$A' = A \cdot \sqrt{\frac{\pi j}{2}} = \sqrt{s\tau_a},$$

Here  $s = j\omega$ , the propagation delay  $\tau_a = a^2(d_t + d_r) / (2d_t d_r c)$  and  $c$  is the speed of light.

Similarly we have

$$\int_0^B \exp(-j\frac{\pi}{2}y^2) dy = \frac{1}{2}(1-j)(1 - \text{erfc}(\sqrt{s\tau_b})). \quad (12)$$

where  $\tau_b = b^2(d_t + d_r) / (2d_t d_r c)$ .

Substitute (11) and (12) into (9) and after some manipulations we can reformulate (9) as

$$H(s) = \frac{1}{2} [1 - (1 - \text{erfc}(\sqrt{s\tau_a})) (1 - \text{erfc}(\sqrt{s\tau_b}))] e^{-s\tau_0}. \quad (13)$$

where  $\tau_0 = d/c$  is the common time delay.

Recall the Laplace transform pair

$$\text{erfc}(\sqrt{s\tau_a}) \stackrel{\text{Laplace}}{\Leftrightarrow} \frac{\sqrt{\tau_a}}{\pi} \frac{1}{t\sqrt{t-\tau_a}} u(t-\tau_a). \quad (14)$$

By applying inverse Laplace transform to (13), its time domain impulse response can be obtained

$$h(t) = \delta(t-\tau_0) * \left[ \frac{1}{2\pi t} \left( \sqrt{\frac{\tau_a}{t-\tau_a}} u(t-\tau_a) + \sqrt{\frac{\tau_b}{t-\tau_b}} u(t-\tau_b) \right) - \frac{\sqrt{\tau_a\tau_b}}{2\pi^2} \left( \frac{u(t-\tau_a)}{t\sqrt{t-\tau_a}} * \frac{u(t-\tau_b)}{t\sqrt{t-\tau_b}} \right) \right]. \quad (15)$$

When  $a \rightarrow \infty, \tau_a \rightarrow \infty$ , (15) reduces to

$$h(t) = \frac{1}{2} \delta(t-\tau_0) * \frac{1}{\pi t} \sqrt{\frac{\tau_b}{t-\tau_b}} u(t-\tau_b), \quad (16)$$

which is exactly the time domain formula for the well-known expression for knife edge diffraction [Jordan and Balmain, (1968), p.503].

Equation (15) consists of three parts. The physical interpretations for the three parts are straightforward. They represent the response from horizontal edge, vertical edge and the mutual interaction between these two edges, respectively.

### 3.2.2 Propagation model based on GTD

Ray concept is used when we attack the diffraction problem with GTD/UTD. The total received field strength is calculated by adding contributions from various rays, which are also referred to as multipath components in the wireless communication. Literature (Mokhtar and Lazaridis, 1999) provides a good GTD-based model in the frequency domain, as our departure point,

$$H(j\omega) = \tilde{D}^{s,h}(j\omega, \psi', \psi) \sqrt{\frac{d_1 + d_1'}{d_1 d_1'}} e^{-jk(d_1 + d_1')} + \tilde{D}^{s,h}(j\omega, \phi', \phi) \sqrt{\frac{d_2 + d_2'}{d_2 d_2'}} e^{-jk(d_2 + d_2')}, \quad (17)$$

where the frequency domain GTD diffraction coefficient for half plane (zero-angle wedge)  $\tilde{D}^{s,h}(j\omega, \psi', \psi)$  can be expressed as

$$\tilde{D}^{s,h}(j\omega, \Omega', \Omega) = -\frac{e^{-j\pi/4} \sqrt{\lambda}}{4\pi} \left[ \frac{1}{\cos\left(\frac{\Omega' - \Omega}{2}\right)} \mp \frac{1}{\cos\left(\frac{\Omega' + \Omega}{2}\right)} \right], \quad (18)$$

The corresponding angle and the distance parameters in (17) and (18) are given by

$$\begin{aligned} \psi' &= \tan^{-1}\left(\frac{d_t}{b}\right) & \psi &= \psi' + \pi + \tan^{-1}\left(\frac{b}{d_t}\right) + \tan^{-1}\left(\frac{b}{d_r}\right) \\ \phi' &= \tan^{-1}\left(\frac{d_t}{a}\right) & \phi &= \psi' + \pi + \tan^{-1}\left(\frac{a}{d_t}\right) + \tan^{-1}\left(\frac{a}{d_r}\right) \end{aligned} \quad (19)$$

$$\begin{aligned} d_1 &= \sqrt{d_t^2 + a^2} & d_1' &= \sqrt{d_r^2 + a^2} \\ d_2 &= \sqrt{d_t^2 + b^2} & d_2' &= \sqrt{d_r^2 + b^2} \end{aligned}$$

To transform (12) to time domain, the key term is the GTD diffraction coefficient, which here can be obtained by setting  $n = 2$  and  $\beta_0 = \pi/2$ , from the GTD solution (8) for wedge diffraction in Section 3.1

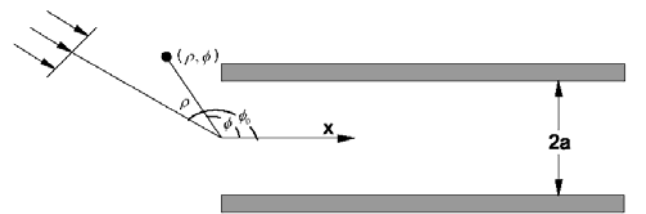
$$D^{s,h}(t, \Omega', \Omega) = \frac{-1}{2\pi} \sqrt{\frac{c}{2}} \left[ \frac{1}{\cos\left(\frac{\Omega - \Omega'}{2}\right)} \mp \frac{1}{\cos\left(\frac{\Omega + \Omega'}{2}\right)} \right] \frac{1}{\sqrt{t}} u(t). \quad (20)$$

We will verify our time domain derivations of two approaches, namely Fresnel-Kirchhoff and GTD, through numerical results in Section 5, where it will be clear that two approaches end up with similar waveform results.

### 3.3 Two parallel half planes model (more than two paths)

Diffraction of a pulse or a transient wave (acoustic or electromagnetic) by a half plane is the earliest diffraction problems. Exact time domain solution of the CIR for such a channel has been obtained by Sommerfeld one century ago. The impulse response for the pulse diffracted by two parallel half planes, is not available in the literature, to the best of our knowledge. Here we will fill this gap. The existing frequency domain solution in the literature is used, as our departing point; the inverse Laplace transform is used to convert the frequency domain solution into time domain. This case is of interest to us since it has multipath components greater than two.

**Figure 5** UWB pulse diffracted by parallel plates



In reality, a lot of environments can be approximately modelled as the problem of diffraction by two parallel PEC planes. Figure 5 illustrates an example. It is assumed that the transmitting antenna is located far away from the edges of two half planes, so that the incident wave can be treated as a plane wave. Moreover, we assume the observation point is also far from these plane edges, so that the distance

parameter  $\rho \rightarrow \infty$ . The incident angle  $\phi_0$  is restricted in the range of  $0 < \phi_0 < \pi$  and the observation angle  $\phi \neq \pi \pm \phi_0$ , which means  $\phi$  is not in the vicinity of the geometrical optics shadow boundary and the reflection boundary. Using the expressions of Bowman et al. (1987), the transfer function for such a channel can be expressed as

$$H(j\omega) = \frac{1}{\sqrt{\pi k p}} e^{j\left(kp + \frac{1}{4}\pi\right)} \frac{2 \sin \frac{1}{2} \phi \sin \frac{1}{2} \phi_0}{\cos \phi + \cos \phi_0} \left[ \begin{aligned} & \cos[ka(\sin \phi + \sin \phi_0)] + \\ & + \frac{1}{\sqrt{4\pi ka}} \left( \frac{1}{\cos \phi} + \frac{1}{\cos \phi_0} \right) \sum_{m=0}^{\infty} \frac{e^{j(2m+1)2ka}}{(2m+1)^{3/2}} \cos[ka(\sin \phi - \sin \phi_0)] - \\ & - \frac{1}{\sqrt{4\pi ka}} \left( \frac{1}{\cos \phi} + \frac{1}{\cos \phi_0} \right) \sum_{m=1}^{\infty} \frac{e^{j(2m)2ka}}{(2m)^{3/2}} \cos[ka(\sin \phi + \sin \phi_0)] + O\left(\frac{1}{ka}\right) \end{aligned} \right] \quad (21)$$

where  $a$  is the distance between two planes. Note that an implicit assumption has been made here is  $ka \gg 1$ , which can be satisfied either if the distance  $a$  is large or the frequency is high.

Taking inversion Laplace transform (by setting  $s = -j\omega$ ), the time domain impulse response can be obtained as

$$h(t) = \left\{ \begin{aligned} & A_0 \frac{u(t)}{\sqrt{t}} * \left[ \frac{\delta(t-a/c(\sin \phi + \sin \phi_0) - \rho/c) +}{\delta(t+a/c(\sin \phi + \sin \phi_0) - \rho/c)} \right] + \\ & A \sum_{m=0}^{\infty} \frac{1}{(2m+1)^{3/2}} u(t) * \left[ \frac{\delta(t-a/c(\sin \phi - \sin \phi_0) - 2(2m+1)a/c - \rho/c) +}{\delta(t+a/c(\sin \phi - \sin \phi_0) - 2(2m+1)a/c - \rho/c)} \right] \\ & - A \sum_{m=1}^{\infty} \frac{1}{(2m)^{3/2}} u(t) * \left[ \frac{\delta(t-a/c(\sin \phi + \sin \phi_0) - 2(2m)a/c - \rho/c) +}{\delta(t+a/c(\sin \phi + \sin \phi_0) - 2(2m)a/c - \rho/c)} \right] \end{aligned} \right\} \quad (22)$$

where

$$A_0 = \frac{\sqrt{2}}{\pi} \frac{1}{\sqrt{\rho/c}} \frac{\sin \frac{1}{2} \phi \sin \frac{1}{2} \phi_0}{\cos \phi + \cos \phi_0} \quad (23)$$

$$A_1 = \frac{1}{\sqrt{2\pi}} \frac{\sin \frac{1}{2} \phi \sin \frac{1}{2} \phi_0}{\cos \phi + \cos \phi_0} \left( \frac{1}{\cos \phi} + \frac{1}{\cos \phi_0} \right) \frac{c}{\sqrt{\rho a}}$$

Physical interpretation for (22) is as follows. The first term in (22) consists of a superposition of edge waves from the two half planes, with the condition that each is excited by the incident pulse alone. The edge wave is characterised by the kernel of  $u(t)/\sqrt{t}$  and can be interpreted with fractional calculus as ‘semi-integral’,

$$f(t) * \frac{u(t)}{\sqrt{t}} = \Gamma(1/2) \cdot D^{-1/2} \{f(t)\}$$

where  $\Gamma(x)$  is the Gamma function and the fractional integral of order  $\gamma$  is defined by Qiu (2006d)

$$D^{-\gamma} \{f(t)\} = \frac{1}{\Gamma(\gamma)} \int_{-\infty}^t (t-\xi)^{\gamma-1} f(\xi) d\xi$$

The second and the third terms are infinite sums, which represent the successive mutual interactions between the two half planes. These two terms are characterised by the kernel of  $u(t)$  and we have

$$f(t) * u(t) = \int_{-\infty}^t f(\xi) d\xi \quad (24)$$

The coefficient  $\frac{1}{(2m+1)^{3/2}}$  or  $\frac{1}{(2m)^{3/2}}$  decreases rapidly as the value of  $m$  is increased. Practically, computation of infinite sums in (22) requires few terms to obtain reasonable accuracy. This will be verified in our numerical results in Section 5.

It should be noted that if both the transmitter antenna and the receiver antenna are located in the canyon between two half planes, then diffraction phenomena is small and multiple reflections dominate the received signal. Time domain CIR for such a channel has been studied in Zhou and Qiu (2006b).

#### 4 Time domain optimum transmit waveform design

Section 2.2 shows that the optimum receiver should be a matched filter matched to the received waveform that is distorted by the channel, not the transmit waveform itself. However, from system point of view, such a matched filter alone is not enough. We can further maximise SNR at the receiver side by carefully designing the transmit waveform (Bell, 1993). The primary difference between the problem in this paper and the standard matched filter problem is the pulse distortion caused by channel. We will show later that if the channel causes no waveform distortion, then the SNR at the receiver side is independent of transmit waveform and thus there is no requirement for optimum transmit waveform.

##### 4.1 Optimum transmit waveform for the channel with pulse waveform distortion

The transmit waveform optimisation problem can be stated as follows. Given the CIR  $h(t)$  and fixed transmitted energy  $E_p$ , we wish to achieve the maximum SNR at the receiver side by a joint design of the transmit waveform and a receiver waveform. This joint optimisation problem caught attention in academia decades ago and has been discussed in Bell (1993) for radar detection.

Assuming the transmitted pulse  $p(t)$  (to be optimised) is confined to the symmetric time interval  $[-T/2, T/2]$ . The energy of transmitted pulse is then

$$E_p = \int_{-T/2}^{T/2} |p(t)|^2 dt. \quad (25)$$

It follows from detection theory that the best receiver to maximise the SNR after the receiver filter is a matched filter

matched to the signal component in  $r(t) = y(t) + n(t)$  in (1): the SNR after such a matched filter is given as

$$SNR = 2E_y / N_0. \quad (26)$$

where  $E_y = \int_{-T/2}^{T/2} |p(t) * h(t)|^2 dt$  is the received signal energy. The problem is then reduced to finding the optimum  $p(t)$  such that  $E_y$  is maximised, under the constraint of fixed  $E_p$ .

It has been shown in Van Trees (1968, p.125) and Bell (1993) that the optimum  $p(t)$  can be obtained by solving the following homogeneous Fredholm integral equation

$$\mu_n \phi_n(t) = \int_{-T/2}^{T/2} \kappa(t-\tau) \phi_n(\tau) d\tau, \quad (27)$$

and let  $p(t) = \phi_0(t)$ , where  $\phi_0(t)$  is the eigenfunction corresponding to the maximum eigenvalue  $\mu_0$ . Here, the time reversal operator  $\kappa(t)$  is defined as  $\kappa(t) = h(t) * h(-t)$ . Without loss of generality, for the eigenvalues  $\mu_n$  corresponding to the eigenfunctions  $\phi_n(\tau)$ , it has been assumed that  $\mu_0 > \mu_1 > \mu_2, \dots$ . An eigenfunction pulse waveform  $\phi_n(t)$  reproduces itself, scaled by a constant  $\mu_0$ , when convolved with the time reversal operator over the interval  $[-T/2, T/2]$ . In other words, an eigenfunction pulse waveform reproduces itself after it propagates through a linear time invaring (LTI) channel with impulse response  $h(t) * h(-t)$ . A time reversal filter  $h(-t)$  can be put in front of the channel  $h(t)$  to form the effective channel of  $h(t) * h(-t)$ , as done in our previous work (Qiu et al., 2006b; Zhou and Qiu, 2006a; Qiu, 2006b; Qiu et al., 2007c; Qiu et al., 2006c; Zhou et al., 2007b; Guo et al., 2007b; Qiu et al., 2007b; Calderon and Qiu, 2007; Qiu et al., 2007a; Zhou et al., 2007a). With optimum  $p(t)$  and  $c(t)$ , we achieve the maximum SNR (after the matched filtering)

$$SNR = 2\mu_0 E_p / N_0. \quad (28)$$

Note that the requirement of optimum information transmission (instead of SNR at the receiver) might result in another transmit waveform. Maximisation of SNR requires the transmitter to put as much as possible energy to the frequency with high transmission capability through the channel, under the fixed transmitted energy constraints, while ignore the other frequency modes with small transmission capability. It is possible that these smaller modes contain a significant quantity of information useful for the system. We consider an extreme case here. When  $T \rightarrow \infty$ , it has been shown in Badhdady (1961, p.360) that all the energy should be placed into one single frequency  $f_{max}$  in the operation band for which  $H(f)$  is the greatest. This leads to a transmit waveform of a sine wave at  $f_{max}$ . However, such a signal of arbitrarily narrow bandwidth

conveys information at a zero rate. Therefore, a trade-off should be made between SNR and information transmission. A chirp signal reflects such a trade-off (Qiu et al., 2007a, 2007b). There is a big performance gap between the chirp waveform and the optimum waveform for modulation (Qiu et al., 2007a, 2007b), in a dense multipath channel. Here, we deal with per-path pulse wave shape distortion – a mechanism different from the dense multipath in Qiu et al. (2007a, 2007b).

To illustrate the principle, we study the optimum transmit waveform for the following channels. One's first thought is to sample (Qiu et al., 2007b) directly, replacing the integral by a summation and solving the resultant set of linear, simultaneous equations for the values of  $\phi_n(t)$  in the interval of  $0 < t < T$ . However, a solution involving delta-function like singularities – which is our case – can hardly be well approximated in this way (Helstrom, 1968). In fact, a continuous solution  $\phi_n(t)$  does not, in general, exist, unless the kernel  $\kappa(t) = h(t) * h(-t)$  has some singularity or the range of integration is unbounded [Helstrom, (1968), p.133].

We will circumvent this singularity problem using a small trick. Practically, all the communication systems are band limited, so we impose such a band pass filter in the system block, to avoid delta-function like singularities in numerical calculation. The transfer function of this filter  $H_F(f)$  is defined as

$$H_F(f) = \begin{cases} 1, & f_1 < |f| < f_2 \\ 0, & \text{otherwise} \end{cases}$$

where  $f_1$  and  $f_2$  are the low and high frequency of the filter, respectively. Its time domain impulse response can be expressed as

$$h_F(t) = 2f_2 \text{sinc}(2f_2 t) - 2f_1 \text{sinc}(2f_1 t) \quad (29)$$

where sinc function is defined as

$$\text{sinc}(t) = \frac{\sin(\pi t)}{(\pi t)}$$

The autocorrelation of the impulse response of this filter can be written as

$$\begin{aligned} & h_F(t) * h_F(-t) \\ &= [2f_2 \cdot \text{sinc}(2f_2 t) - 2f_1 \cdot \text{sinc}(2f_1 t)] \\ & \quad * [2f_2 \cdot \text{sinc}(-2f_2 t) - 2f_1 \cdot \text{sinc}(-2f_1 t)] \\ &= 2f_2 \cdot \text{sinc}(2f_2 t) + 2f_1 \cdot \text{sinc}(2f_1 t) - 4f_1 \cdot \text{sinc}(2f_1 t) \\ &= h_F(t) \end{aligned} \quad (30)$$

It is shown that autocorrelation of the function of  $h_F(t)$  reproduces itself. For cognitive radio purpose (Fette, 2006), the frequency response of this filter could be in an arbitrary passband (e.g.,  $k$ th element subband) located under the FCC spectral mask (3.1 GHz – 10.6 GHz) (Zhang et al., 2006). Assuming the CIR of a specific channel  $h_c(t)$ , then the overall of the CIR will be  $h(t) = h_F(t) * h_c(t)$ .

### 4.1.1 Wedge channel

Consider a case that LOS is blocked by a PEC wedge, which is illustrated in Figure 1. The CIR of such an ideal wedge channel (implying an infinite bandwidth) can be expressed as

$$h_c(t) = \sqrt{\frac{c}{2t}} \cdot \frac{\sin \frac{\pi}{n}}{n\pi \sin \beta_0} \cdot \left[ \frac{1}{\cos \frac{\pi}{n} - \cos \left( \frac{\phi - \phi'}{n} \right)} \mp \frac{1}{\cos \frac{\pi}{n} - \cos \left( \frac{\phi + \phi'}{n} \right)} \right] \cdot u(t) \quad (31)$$

$$= C(n, \beta_0, \phi, \phi') \cdot \frac{u(t)}{\sqrt{t}}$$

where

$$C(n, \beta_0, \phi, \phi') = \sqrt{\frac{c}{2}} \frac{\sin \frac{\pi}{n}}{n\pi \sin \beta_0} \cdot \left[ \frac{1}{\cos \frac{\pi}{n} - \cos \left( \frac{\phi - \phi'}{n} \right)} \mp \frac{1}{\cos \frac{\pi}{n} - \cos \left( \frac{\phi + \phi'}{n} \right)} \right]$$

is a time-independent constant whose value depends on the environment. The autocorrelation of the above CIR in (31) is given by

$$h_c(t) * h_c(-t) = C^2 \cdot \frac{u(t)}{\sqrt{t}} * \frac{u(-t)}{\sqrt{-t}}$$

Then, the autocorrelation of the overall CIR for a band-passed wedge channel is written as

$$\begin{aligned} \kappa(t) &= h_c(t) * h_c(-t) * h_F(t) * h_F(-t) \\ &= C^2 \cdot \chi_1(t) * \chi_1(-t) \end{aligned} \quad (32)$$

where  $\chi_1(t) = u(t) / \sqrt{t} * h_F(t)$ . Substituting (32) into (27) and solve (27) for  $\phi(t)$  numerically, we can obtain the optimum waveform for wedge channels. The numerical calculation of the singular function  $\chi_1(t)$  will be shown in Section 5.1.

### 4.1.2 Rectangular building channel

The time domain CIR for such a channel has been derived in Section 3.2. It follows from equation (15) that the CIR consists of three parts. Practically, the contribution from the third part (mutual interaction between two edge waves) in (15) is very weak and could be ignored. Mathematically, the CIR of (15) can be approximated by the first two parts

$$\begin{aligned} h(t) &\approx \frac{\sqrt{\tau_a}}{2\pi} \cdot \frac{1}{(t + \tau_a)\sqrt{t}} u(t) * \delta(t - \tau_a) \\ &+ \frac{\sqrt{\tau_b}}{2\pi} \cdot \frac{1}{(t + \tau_b)\sqrt{t}} u(t) * \delta(t - \tau_b) \end{aligned} \quad (33)$$

where the common time delay  $\tau_0$  has been ignored, without loss of generality of the final numerical results for optimum waveforms.

In Laplace transform, it is known that the high frequency asymptotic response as  $f \rightarrow \infty$  is determined by transient early time response as  $t \rightarrow 0^+$ . For the term of  $\frac{1}{(t + \tau_{a,b})\sqrt{t}}$ , the energy is concentrated in the

neighbourhood of  $t \rightarrow 0^+$ . The asymptotic limit of this function can be investigated, instead, to simplify the analysis and gain insight. It has been shown in (10) that the use of this asymptotic limit to approximate the edge diffraction causes no difference to the exact solution. Therefore, for high frequency [i.e.,  $f_{1,2}$  in (29) is large], we

have  $\frac{1}{(t + \tau_{a,b})\sqrt{t}} \approx \frac{1}{\tau_{a,b}\sqrt{t}}$ . With this approximation, (33)

can be further expressed in the form of

$$h(t) \approx C_a \frac{u(t)}{\sqrt{t}} * \delta(t - \tau_a) + C_b \frac{u(t)}{\sqrt{t}} * \delta(t - \tau_b) \quad (34)$$

where  $C_a = \frac{1}{2\pi\sqrt{\tau_a}}$  and  $C_b = \frac{1}{2\pi\sqrt{\tau_b}}$ . With (34), the time

reversal operator  $\kappa(t)$  for such a rectangular plate channel can be expressed as

$$\begin{aligned} \kappa(t) &\approx (C_a^2 + C_b^2) \cdot \chi_1(t) * \chi_1(-t) + \\ &C_a C_b \cdot \chi_1(t) * \chi_1(-t) \\ &* \{ \delta(t - \tau_a + \tau_b) + \delta(t - \tau_b + \tau_a) \} \end{aligned} \quad (35)$$

For a special case when the width of the building is twice as its height, i.e.,  $a = b$ , then the time reversal operator  $\kappa(t)$  can be simplified in the form of

$$\kappa(t) \approx 4C_a^2 \cdot \chi_1(t) * \chi_1(-t) \quad (36)$$

It is interesting to note that the optimum transmit waveform for such a channel is the same as a wedge channel studied in Section 4.1.1.

### 4.1.3 Two half planes waveguide channel

As stated earlier in Section 3.3, the half plane waveguide model is a little more complicated than the other two models studied in this paper, due to the existence of multiple diffraction (caused by waveguide edges). However, we can simplify the problem by focusing on the main lobe of the  $\kappa(t)$ , instead of the whole  $\kappa(t)$ . Given the CIR  $h(t)$  derived in (22), the main lobe of  $\kappa(t)$  for two half planes channel can be approximated as

$$\begin{aligned} \kappa(t) &\approx 2A_0^2 \cdot \chi_1(t) * \chi_1(-t) \\ &+ 2A_1^2 \cdot \left\{ \sum_{m=1}^{\infty} m^{-3} \right\} \cdot \chi_2(t) * \chi_2(-t) \end{aligned} \quad (37)$$

where  $\chi_2(t) = u(t) * h_F(t)$ . Considering the convolution property of  $u(t)$  shown in (24), closed-form expression for  $\chi_2(t) * \chi_2(-t)$  can be derived as follows

$$\begin{aligned} \chi_2(t) * \chi_2(-t) &= u(-t) * \left\{ \int_{-\infty}^t h_F(\xi) d\xi \right\} \\ &= u(-t) * \{ Si(2\pi f_1 t) / \pi - Si(2\pi f_2 t) / \pi \} \\ &= u(-t) * \{ -Si(-2\pi f_1 t) / \pi + Si(-2\pi f_2 t) / \pi \} \end{aligned} \quad (38)$$

Here, the sine integral function  $Si(x)$  is defined as

$$Si(x) = \int_0^x \frac{\sin(t)}{t} dt$$

Note that  $Si(x)$  is an odd function and can be implemented with a Matlab built-in function. The closed-form expression for the integral of  $Si(x)$  is written as

$$\int Si(t) dt = \cos(t) + t \cdot Si(t)$$

Thus, we have

$$\begin{aligned} \chi_2(t) * \chi_2(-t) &= \\ &= \frac{\cos(2\pi f_2 t)}{2\pi^2 f_2} - \frac{\cos(2\pi f_1 t)}{2\pi^2 f_1} + \frac{t}{\pi} \cdot [Si(2\pi f_2 t) - Si(2\pi f_1 t)] \end{aligned} \quad (39)$$

Note that the general solution for such a model is still open. The delay spread is too big, such that the sampling points are too big for the computer to handle. Some alternative approach has to be found to overcome this problem. More analytical treatment about the series in (22) is needed to retain only the leading terms; then closed-form expressions can be derived from these leading terms. Further results will be reported elsewhere.

## 4.2 Numerically computing eigenfunctions

Except for some classical cases such as band limited signals (Van Trees, 1968; Bell, 1993), the eigenfunctions and eigenvalues are generally difficult to be solved in a closed-form. In this section we are interested in computing the eigenfunctions and eigenvalues numerically. The idea is to sample the function waveform and borrow the powerful matrix theory to solve the problem. We firstly sample the autocorrelation function  $\kappa(t)$  with sufficiently high sampling rate such that all the significant channel frequencies are included.

As treated in Section 4, the optimal pulse waveform (maximising SNR) is, according to Qiu et al. (2007b), a solution to the integral function

$$\mu_n \cdot \phi_n(t) = \int_{-T/2}^{T/2} \kappa(t-\tau) \phi_n(\tau) d\tau \quad n=1, \dots, \infty, \quad (40)$$

After sampling  $t = m\Delta t$ , where  $\Delta t$  is sampling time with a total of  $2N+1$  samples, (40) becomes

$$\mu_n \cdot \begin{bmatrix} \phi_n(-N) \\ \phi_n(-N+1) \\ \vdots \\ \phi_n(N) \end{bmatrix} = \begin{bmatrix} \kappa(-2N) & \cdots & \kappa(0) \\ \kappa(-2N+1) & \cdots & \kappa(1) \\ \vdots & \ddots & \vdots \\ \kappa(0) & \cdots & \kappa(2N) \end{bmatrix} \begin{bmatrix} \phi_n(-N) \\ \phi_n(-N+1) \\ \vdots \\ \phi_n(N) \end{bmatrix} \quad (41)$$

We, then, transform the integral function to a matrix problem. The solution of the integral function (40) is equivalent to finding the eigenvector of matrix  $K$  with dimensions  $((2N+1) \times (2N+1))$ , containing values of  $\kappa(t)$  at  $t = m\Delta t$  in (41). Several remark notes can be drawn from (41)

- The optimum waveform obtained via the numerical solution introduced above is not necessarily the unique one; though the maximum eigenvalue is unique, the corresponding eigenfunction (eigenvector) might not.
- If there is no per-path pulse distortion (e.g., free space transmission), the time reversal operator  $\kappa(t) = \alpha_0 \delta(t - \tau_0)$ , where  $\alpha_0$  and  $\tau_0$  are the constants depending on the distance between the transmitter and the receiver. For this special case, there is no need for solving for optimum transmit waveforms, since any waveform will reproduce itself after being convoluted with this time reversal operator.
- We can improve computation accuracy by decreasing sampling interval  $\Delta t$ . The selection of  $\Delta t$  must satisfy the Nyquist condition  $1/\Delta t \geq 2(f_2 - f_1)$ , where  $f_2 - f_1$  is the bandwidth of the signal.

It is also evident that the availability of time domain CIR  $h(t)$  [and thus its time reversal operator  $\kappa(t)$ ] is critical to computing the optimum waveform  $\phi_0(t)$ .

## 5 Numerical results

### 5.1 Calculation of singularity in the impulse response of wedge diffraction

A singularity appears in the impulse response for most of channels where diffraction phenomena is involved, e.g., in equation (6) (wedge diffraction), when  $t \rightarrow 0$ , then  $D^{s,h}(t) \rightarrow \infty$ , thus in equation (4), there is a singularity at  $t = 0$ . How to numerically calculate this singularity is not a trivial issue. Since the singularity is exactly where the energy concentrates (and also defines the type of the pulse distortion), it cannot be directly removed using the time windowing. From an electromagnetic point of view, this singularity at the diffracted wavefront is essential. An integral-differential (*int-diff*) approach has been proposed and proved to be an efficient way to remove this discontinuity at  $t = 0$  during the calculation (Qiu et al., 2005c). In this section, we will further verify this approach by comparing it with the more exact approach called analytic time transform (Rousseau and Pathak, 1996).

### 5.1.1 Int-diff approach

Mathematically, the principle of this int-diff approach can be described as follows,

$$\int_0^t [p(t) * g(t)] dt = p(t) * \int_0^t g(t) dt \quad (42)$$

hence, we have

$$p(t) * g(t) = \frac{d}{dt} \left[ p(t) * \int_0^t g(t) dt \right] \quad (43)$$

where  $g(t)$  has a singularity in the time domain. The integration  $\int_0^t g(t) dt$  removes the singularity and can often be obtained in a closed-form. The reason why we call this approach *int-diff* approach is because additional integration and differentiation operation are involved to get the convolution result.

Again, we consider the wedge diffraction case as an example. Notice that the singularity in (4) is solely caused by term  $F(X_m, t)$ . We will focus on this term first. The rest of work is just linear summation. According to *int-diff* approach, firstly we will need to integrate  $F(X_m, t)$ . Happily, we have a closed-form for the integration of  $F(X_m, t)$ , which can be expressed as

$$\begin{aligned} \bar{F}(X_m, t) &= \int_0^t F(X_m, t) dt \\ &= 2\sqrt{\frac{X_m}{\pi}} \operatorname{atan} \left( \sqrt{\frac{ct}{X_m}} \right) \end{aligned} \quad (44)$$

Let  $\bar{D}^{s,h}(t)$  denotes the integration of the wedge diffraction coefficient  $D^{s,h}(t)$ , then we have

$$\bar{D}^{s,h}(t) = \frac{-1}{2n\sqrt{2\pi\sin\beta_0}} \sum_{m=1}^4 K_m^{s,h} \bar{F}(X_m, t) \quad (45)$$

Note that singularity in  $D^{s,h}(t)$  has been removed in the new integration expression  $\bar{D}^{s,h}(t)$ . The latter can be used to do the convolution, followed by a differentiation operation as a compensation.

### 5.1.2 Analytic time transform (ATT)

ATT is another classic technique used to perform an efficient convolution with a broad class of excitation pulse functions. In this paper, this classic approach will be briefly introduced and serve as a benchmark for the *int-diff* approach.

The second version ATT in Rousseau and Pathak (1996) is defined as

$${}_f^+(t) = \frac{j}{\pi} \int_{-\infty}^{\infty} \frac{f(\tau)}{t - \tau} d\tau, \text{ for } \operatorname{Im}(t) > 0 \quad (46)$$

Here,  $f(t)$  is an arbitrary function. The '+' sign over  $f$  means an analytical signal in a complex-time domain. Let  $p(t)$  and  $h(t)$  denote the incident pulse and the impulse response of the system, respectively. Then we have,

$$p(t) * h(t) = \frac{1}{2} \operatorname{Re} \left[ {}_p^+(t) * {}_h^+(t) \right] \quad (47)$$

Notice that the singularity on real time axis ( $\operatorname{Im}(t) = 0$ ) in  ${}_h^+(t)$  is only a branch point singularity and not a pole. Therefore, the difficulty in calculation of the singularity in  $h(t)$  has been removed by ATT in  ${}_h^+(t)$ . Moreover, if we choose the incident pulse such that in the frequency domain  $p(\omega)$  can be modelled, using exponentials, as

$$p(\omega) = \sum_{n=1}^N A_n e^{-\alpha_n \omega} \text{ for } \omega > 0 \quad (48)$$

or equivalently, in time domain

$${}_p^+(t) = \sum_{n=1}^N A_n \delta^+(t + j\alpha_n) \quad (49)$$

where  $\delta(t)$  is Dirac delta function. Then the convolution can be evaluated in closed-form as

$$p(t) * h(t) = \operatorname{Re} \left[ \sum_{n=1}^N A_n {}_h^+(t + j\alpha_n) \right] \quad (50)$$

where the shifting property of the analytic delta function

$$\frac{1}{2} \delta^+(t + j\alpha_n) * {}_h^+(t) = {}_h^+(t + j\alpha_n) \quad (51)$$

has been used.

To verify our result with *int-diff* approach, we use the same incident pulse as used in Rousseau and Pathak (1996). Mathematically, the frequency domain of the incident pulse  $p(\omega)$  is defined by

$$p(\omega) = C_0 (1 - e^{-\omega T})^{P_1} e^{-\omega P_2 T} \quad (52)$$

where  $T = \frac{1}{2\pi f_c} \ln \left( \frac{P_1 + P_2}{P_1} \right)$ ,  $f_c$  represents the centre

frequency, which can be adjusted easily according to different requirements. The peak of the  $p(\omega)$  is normalised

by choosing  $C_0 = \left( \frac{P_1 + P_2}{P_1} \right)^{P_1} \left( \frac{P_1 + P_2}{P_1} \right)^{P_2}$ . Time domain

waveform of the incident pulse can be conveniently obtained by

$$p(t) = \operatorname{Re} \left[ {}_p^+(t) \right] = \operatorname{Re} \left[ \frac{j}{\pi} \sum_{n=0}^{P_1} \frac{C_0 \binom{P_1}{n}}{t + j(n + P_2)T} \right] \quad (53)$$

where  $\binom{P_1}{n} = \frac{P_1!}{n!(P_1 - n)!}$ .

Let  $D^+(t)$  denote the analytic impulse response of wedge diffraction, then using the convolution property in Table 2.1 in Rousseau and Pathak, (1996), the received pulse will be

$$\begin{aligned} r(t) &= \text{Re} \left[ \frac{1}{2} p^+(t) * D^+(t) \right] \\ &= \text{Re} \left[ \sum_{n=0}^{P_1} C_0 \binom{P_1}{n} D^+(t + j(n + P_2)T) \right] \end{aligned} \quad (54)$$

Instead of integration, the ATT approach removes the singularity by performing an analytic transform. The analytic transform of a time domain function is not so straightforward, especially when the function itself is complicated. According to Rousseau and Pathak, (1996), the analytic wedge diffraction coefficient  $D^+(t)$  can be expressed as

$$D^{s,h}(t) = \frac{-1}{2n\sqrt{2\pi}\sin\beta_0} \sum_{m=1}^4 K_m^{s,h} F^+(x_m, t) \quad (55)$$

where

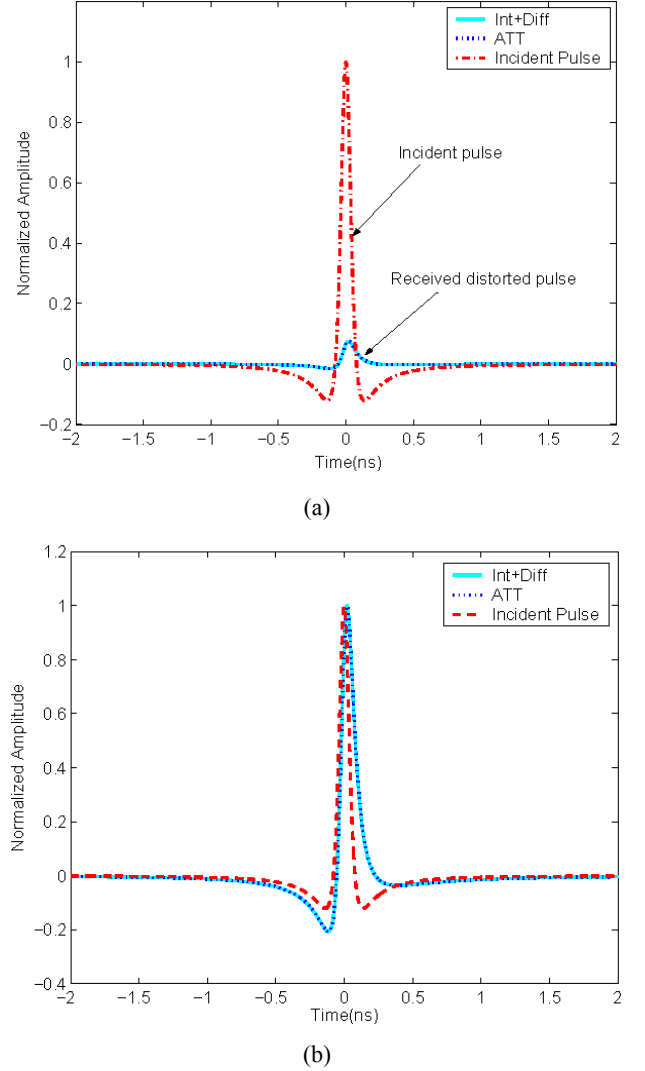
$$F^+(x_m, t) = \frac{\sqrt{x_m / \pi}}{\sqrt{-jt}(\sqrt{-jt} + \sqrt{jx_m / c})} \quad (56)$$

and the rest of the parameters are the same with that of TD-UTD, presented in Section 3.1.

Figure 6 shows the received waveforms, calculated with ATT and *int-diff* approaches, respectively. The incident waveform, marked as red slash curve, is also plotted, as a reference. Firstly, it is found that the received waveforms, calculated with different approaches, are in excellent agreement. Secondly, it can also be observed from Figure 6(a) that the diffracted pulse is much weaker than the incident pulse, due to the huge energy loss caused by diffraction. To better compare the waveform between incident pulse and the diffracted pulse, their amplitudes are scaled to the same value and their waveforms are shown in Figure 6(b). It is evident that the diffracted pulse waveform is much different from the incident one, indicating a pulse wave shape distortion caused by diffraction.

The parameters used in our simulation are as follows: For the incident pulse,  $P_1 = 2, P_2 = 1$  and  $f_c = 2$  GHz. The parameters for the wedge are:  $\beta_0 = \pi/2$ ,  $n = 3/2$ ,  $\phi = 5\pi/6$ ,  $\phi' = \pi/3$  and the soft boundary condition has been considered.

**Figure 6** Waveform comparison between the int-diff and the ATT approach (a) incident pulse and the received pulse (b) waveform comparison (see online version for colours)



Notes: In (a) amplitudes have been normalised to the incident pulse to compare the power of the incident pulse and the received pulse. In (b), the incident pulse has been scaled to the same amplitude of the received pulse to compare their waveforms.

## 5.2 Rectangular building

For all the figures (unless otherwise specified) in this paper, the waveform labelled 'TD' is obtained by convolution of the incident pulse  $p(t)$  with the time domain CIRs derived in this paper and the waveform labelled 'FD+IFFT' is obtained by applying IFFT of the product of  $P(f)H(f)$ , where  $P(f)$  and  $H(f)$  are Fourier transform of  $p(t)$  and channel transfer function, respectively. We have verified our time domain derivation by showing good agreements between 'TD' results and their corresponding 'FD+IFFT' results.

In the following numerical results, we choose the second order derivative of Gaussian pulse as the incident pulse, which mathematically is defined as

$$p(t) = \left[ 1 - 4\pi \left( \frac{t - t_c}{w} \right)^2 \right] e^{-2\pi \left( \frac{t - t_c}{w} \right)^2} \quad (57)$$

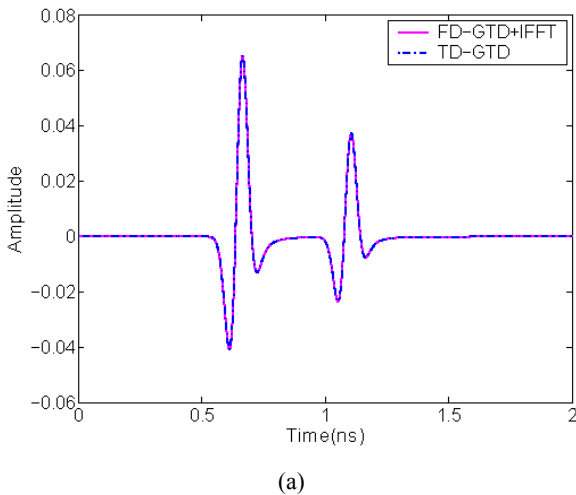
where  $w$  is the parameter controlling the width of the pulse (and therefore the frequency bandwidth of the transmit signal) and  $t_c$  is time shift to put the pulse in the middle of the window.

Figure 7 shows a comparison between GTD and Fresnel-Kirchhoff models. Here, we set  $w = 0.1$  ns and  $t_c = 0.3$  ns. The environment parameters used in the simulation are as follows:  $d_t = 1000$  m,  $d_r = 900$  m,  $a = 15$  m and  $b = 10$  m. Several observations can be made from Figure 7:

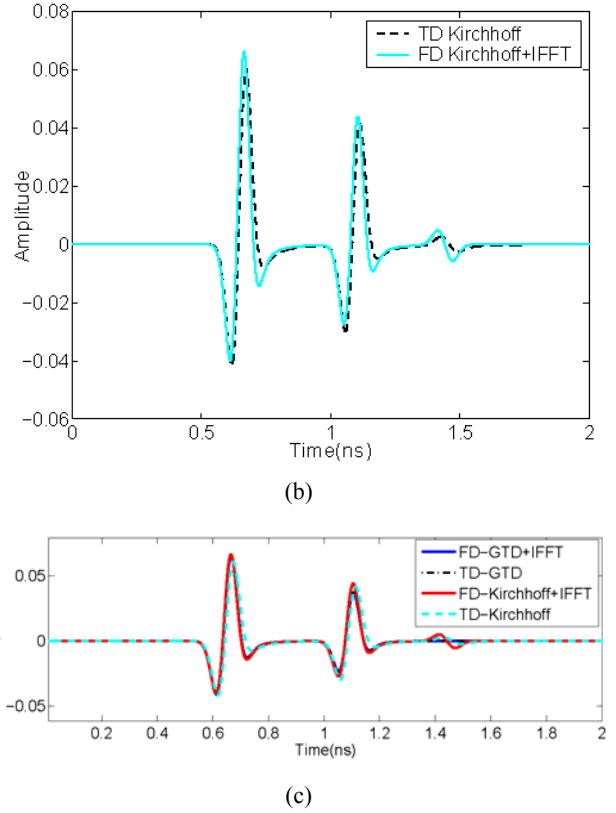
- For both GTD model and Fresnel-Kirchhoff models, time domain results show very good agreement with the results transformed from the frequency domain via IFFT (labelled 'FD+IFFT'). This verifies our time domain derivation.
- The diffracted waveforms based on GTD approach and Fresnel-Kirchhoff approach agree very well to each other, except that the Fresnel-Kirchhoff result has an additional small waveform response. This extra 'baby response' can be identified from its time domain formula to be the mutual interaction (coupling) term between two edges, which has not been taken into account by the GTD-based model.

Note that in the simulation results shown in Figure 7, common propagation delays has been neglected, for the convenience of comparison.

**Figure 7** Simulated pulse waveforms after a second order derivative of Gaussian pulse passes through a rectangular channel described in Figure 4, (a) GTD (b) Kirchhoff (c) comparison Kirchhoff and GTD results (see online version for colours)



**Figure 7** Simulated pulse waveforms after a second order derivative of Gaussian pulse passes through a rectangular channel described in Figure 4, (a) GTD (b) Kirchhoff (c) comparison Kirchhoff and GTD results (continued) (see online version for colours)

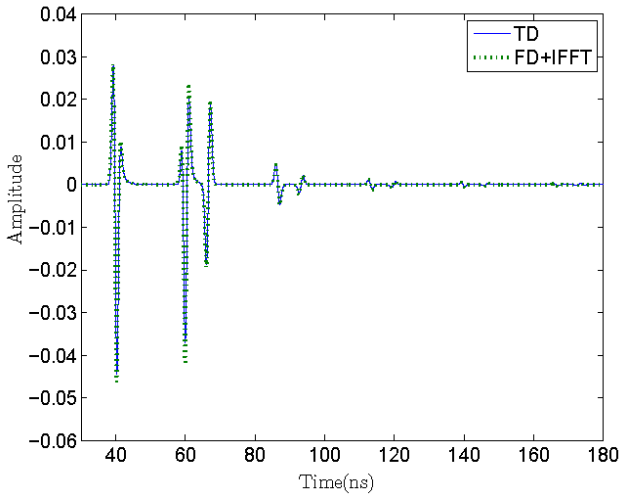


### 5.3 Two parallel half planes model

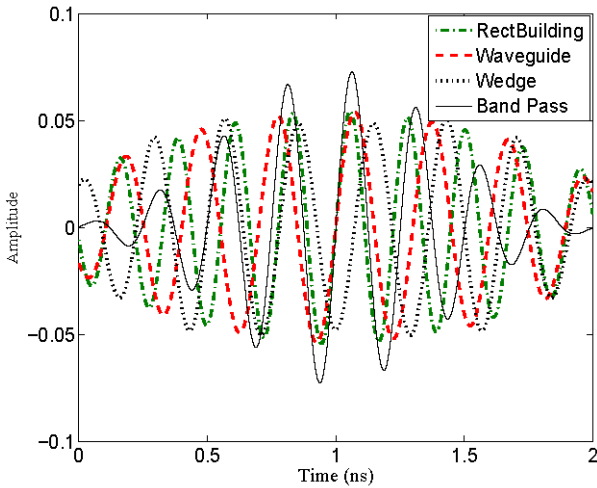
As mentioned in Section 3.3, when a UWB pulse is incident on the parallel half plane channel, the received signal consists of three parts, with each part including two identical (but separated in time) signal components. The relative signal strengths of these three parts depend on the values of the coefficient  $A_0$  and  $A_1$ , which in turn depend on the environment and the location of the antenna. Figure 8 shows the received signal when a second order derivative of Gaussian pulse is incident on the parallel half plane channel. The incident pulse width is  $w = 2$  ns. The geometrical parameters for parallel planes are as follows:  $\rho = 20$  m,  $\phi = 8/15\pi$ ,  $\phi_0 = 5/6\pi$ ,  $a = 2$  m.

It can be seen from Figure 8 that the waveforms of the received pulses are not the second order derivative Gaussian (the transmitted pulse). It follows from Section 3.3 that they are actually 'semi-integral' (or integral) forms of the second order derivative Gaussian pulse. Again, the agreement between the waveform obtained by time domain convolution (labelled 'TD') and frequency domain result (labelled 'FD+IFFT') shows our time domain closed-form derivation is correct. Additionally, although equation (22) shows infinite terms, it is seen from Figure 8 that these sums converge very quickly.

**Figure 8** UWB pulse diffracted by a two-half-plane waveguide (see online version for colours)



**Figure 9** Optimum transmit waveform design for different propagation channels. The energy of each waveform has been normalised (see online version for colours)



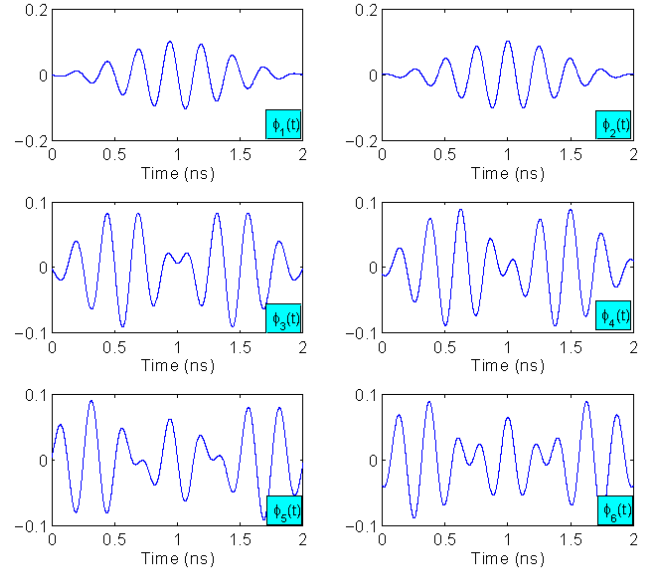
#### 5.4 Optimum transmit waveform design

Figure 9 shows the optimum transmit waveforms for the different propagation channels, namely, the wedge channel (labelled ‘wedge’) studied in Section 3.1, the rectangular building channel (labelled ‘rectbuilding’) studied in Section 3.2, the two half planes waveguide channel (labelled ‘waveguide’) studied in Section 3.3 and the band pass channel (labelled ‘band pass’). Here band pass channel is a free space channel (no diffraction mechanism involved) but only let selected frequency band pass through. The optimum waveforms have been obtained by substituting  $\kappa(t)$  of corresponding channels into (41) and numerically computing  $\phi(t)$  associated with the maximum eigenvalue.

A comparison of these waveforms shows that frequency selectivity determined by the physical process of diffraction does have critical impact on modulation waveform optimisation. For the convenience of waveform comparison, the energy of the computed optimum transmit waveforms

( $\phi(t)$ ) for different channels have been normalised. The parameters used in the simulation are as follows:  $T = 2$  ns,  $f_1 = 3$  GHz,  $f_2 = 5$  GHz. In each model, the environmental parameters used to calculate the optimum waveform are the same as those used for the computation of the distorted receiving waveforms in this section.

**Figure 10** The first six eigen waveforms for a band pass channel (see online version for colours)



For the purpose of maximising the SNR at the receiver side, all the energy should be sent through the optimum transmit waveform, which is the eigenfunction associated with the maximum eigenvalue of  $\kappa(t)$ . For the purpose of flexibility, however, we are interested in transmission of a linear combination of the eigenfunctions whose eigenvalues are close to the maximum one. Figure 10 shows the first six eigen waveforms for the ideal passband channel with  $WT = 4$ . Their corresponding eigenvalues are 1.0000, 0.9999, 0.9979, 0.9976, 0.9621 and 0.9599. We can also transmit these waveforms, in parallel, to increase the data rate. Note that the eigenfunctions for the low pass channel (which can be viewed as a special case of the bandpass channel discussed in this paper when  $f_1 = 0$ ) is known as prolate spheroidal wave functions (Slepian and Pollak, 1961) and has been proposed as a novel UWB pulse shaping technique in Dilmaghani et al. (2003).

## 6 Conclusions

The motivation of this work is to understand the implication of the ultra-wide bandwidth in the context of modulation pulse waveforms. The derivation of the closed-form CIR for the canonical channels, including wedge, rectangular plate and two parallel half planes, is of fundamental significance to time domain channel modelling. In contrast with the narrowband modelling, transient electromagnetic analysis is required.

The resultant expressions are used to calculate the optimum modulation waveforms. Some interesting results are obtained: frequency selectivity determined by the physical process of diffraction does have critical impact on modulation waveform optimisation. More important, for short pulses of duration (e.g., of two nanoseconds), the optimum waveforms are not sinusoidal. It is well known that, when the pulse duration becomes infinite, the optimum waveforms, i.e., the eigenfunctions of the kernel, will become sinusoidal – thus justification for orthogonal frequency division multiplexing (OFDM). The eigenfunctions of the kernel (being sinusoidal) for narrowband systems are always identical, but with different frequencies (tones) for these sinusoidal eigenfunctions. The optimisation needed is the power allocation for each tone. The transient UWB pulses, on the other hand, require more optimisation: the waveform families are not known in general, but needs numerical calculation (as a functional of the CIR through the kernel of the Fredholm integral equation). This fundamental observation appears to suggest that the transmission for impulsive short pulses (of ultra-wide bandwidth) is fundamentally different from that of narrowband communication systems using (asymptotically) infinitely long pulses (of narrow bandwidth). Using some canonical channels as examples, this paper paves the way for understanding this conceptual difference between two types of wireless communications systems.

Singularity caused by light diffraction is the dominant mechanism for imaging – this reflects the success of JPEG-2000 for imaging compression standard, since wavelet representation is ideal for such point singularities. UWB communication is analogous to imaging in some sense. As a result, the edge diffraction of a short pulse is fundamental to UWB communication. One interesting property of the UWB signal is its compressibility (Candes and Romberg, 2004) – due to the isolated singularity of  $\frac{1}{\sqrt{t}}u(t)$  in the impulse response seen in Section 5.1; we can find a basis (e.g., wavelet) in which the expansion coefficients of these signals decay rapidly. This unique property of a diffracted UWB signal has a natural connection with compressed sampling (Candes and Wakin, 2008). As seen in Section 5.1, uniform sampling using Shannon's sampling theorem is infeasible since the signal has infinite bandwidth. A systematical investigation of this link with compressing sampling/sensing is ongoing and the results will be reported elsewhere.

Finally, the physics-based channel modelling is critical to understanding the fundamental limits of a UWB communication system. An empirical model cannot capture all the information of physical signals.

## Acknowledgements

This work is funded by the Office of Naval Research through a grant (N00014-07-1-0529), National Science Foundation through a grant (ECS-0622125), the Army Research Laboratory and the Army Research Office through a STIR grant (W911NF-06-1-0349) and a DURIP grant (W911NF-05-1-0111) and ONR Summer Faculty Fellowship Program Award. We thank Drs. Brian Sadler, Santanu K. Das and Robert Ulman for helpful discussions.

## References

- Badhdady, E.J. (1961) *Lectures on Communications System Theory, Ch. 14*, McGraw-Hill, New York.
- Bell, M.R. (1993) 'Information theory and radar waveform design', *IEEE Trans. on Inf. Theory*, September, Vol. 39, No. 5, pp.1578–1597.
- Bowman, J.J., Senior, T.B.A. and Uslenghi, P.L.E. (1987) *Electromagnetic and Acoustic Scattering by Simple Shapes*, Hemisphere, New York.
- Calderon, M. and Qiu, R.C. (2007) *Time Reversal for Ultra-wideband (UWB) Sensor Networking*, Tech. Rep., Final Report to Army Research Office, Grant No. W911NF-06-1-0349, 151 pages, TTU, Cookeville, TN, July.
- Candes, E.J. and Romberg, J. (2004) 'Practical signal recovery from random projections', *Wavelet Applications in Signal and Image Processing XI, Proc. SPIE Conf.* 5914.
- Candes, E.J. and Wakin, M.B. (2008) 'An introduction to compressive sampling', *IEEE Sig. Mag.*, March, pp.21–30.
- Dilmaghani, R.S., Ghavami, M., Allen, B. and Aghvami, H. (2003) 'Novel UWB pulse shaping using prolate spheroidal wave functions', *Proc. 14th IEEE International Symposium on Personal, Indoor and Mobile Radio Communications (PIMRC 2003)*, Beijing, September, pp.602–606.
- Fette, B. (2006) *Cognitive Radio Technology*, Elsevier, UK.
- Guo, N., Sadler, B.M. and Qiu, R.C. (2007a) 'Reduced-complexity time reversal enhanced autocorrelation receivers considering experiment-based UWB channels', *IEEE Trans. Wireless Comm.*, Vol. 6, No. 12, pp.4221–4226.
- Guo, N., Zhang, Q., Qiu, R.C. and Mo, S. (2007b) 'UWB MISO time reversal with energy detector receiver over ISI channels', *4th Annual IEEE Consumer Communications and Networking Conference, CCNC'07*, Las Vegas, Nevada, January.
- Helstrom, C.W. (1968) *Statistical Theory of Signal Detection*, 2nd ed., Pergamon, New York.
- Jordan, E.C. and Balmain, K.G. (1968) *Electromagnetic Waves and Radiating Systems*, 2nd ed., Prentice-Hall.
- Kouyoumjian, R.G. and Pathak, P.H. (1974) 'A uniform geometric theory of diffraction for an edge in a perfectly conducting surfaces', *Proc. IEEE*, November, Vol. 62, pp.1448–1461.
- Mokhtaris, H. and Lazaridis, P. (1999) 'Comparative study of lateral profile knife-edge diffraction and ray tracing technique using GTD in urban environment', *IEEE Tran. Veh. Tech.*, January, Vol. 48, No. 1, pp.255–261.
- Molisch, A. (2004) *Status of Models for UWB Propagation Channel*, IEEE 802.15.4a Channel Model (Final Report), August.

- Qiu, R.C. (1996) *Digital Transmission Media: UWB Wireless Channel, MMIC and Chiral Fiber*, PhD Thesis, January, Polytechnic University, Brooklyn, NY.
- Qiu, R.C. (2002) 'A study of the ultra-wideband wireless propagation channel and optimum UWB receiver design (Part 1)', *IEEE J. Selected Areas in Commun. (JSAC), The First JSAC Special Issue on UWB Radio*, December, Vol. 20, pp.1628–1637.
- Qiu, R.C. (2004) 'A generalized time domain multi-path channel and its application in ultra-wideband (UWB) wireless optimal receiver design: part II wave-based system analysis', *IEEE Trans. Wireless Communications*, November, Vol. 3, No. 11, pp.2312–2324.
- Qiu, R.C. (2005) 'Optimum and sub-optimum detection of physics-based UWB signals', *Dynamics of Continuous, Discrete and Impulsive Systems – An International Journal for Theory and Applications (Series B)*, Vol. 12, No. 3, pp.321–334.
- Qiu, R.C. (2006a) 'A generalized time domain multi-path channel and its application in ultra-wideband (UWB) wireless optimal receiver design: part 3 system performance analysis', *IEEE Trans. Wireless Communications*, Vol. 5, No. 10.
- Qiu, R.C. (2006b) 'A theory of time-reversed impulse multiple-input multiple-output (MIMO) for ultra-wideband (UWB) communications (invited paper)', *2006 Int'l Conf. UWB*, October.
- Qiu, R.C. (2006c) 'Propagation effects', book chapter, in M. Di Benedetto, T. Kaiser, A.F. Molisch, I. Oppermann, C. Politano and D. Porcino (Eds.): *UWB Communication Systems: A Comprehensive Overview*, Hindawi Publishing, New York.
- Qiu, R.C. (2006d) 'UWB pulse propagation and detection', book chapter, in X. Shen, M. Guizani, R.C. Qiu, T. Le-Ngoc (Eds.): *UWB Wireless Communications*, John Wiley, New York.
- Qiu, R.C. and Lu, I.T. (1999) 'Multipath resolving with frequency dependence for broadband wireless channel modelling', *IEEE Trans. Veh. Tech.*, January, Vol. 48, pp.273–285.
- Qiu, R.C., Liu, H.P. and Shen, X. (2005a) 'Ultra-wideband for multiple access', *IEEE Commun. Mag.*, February, Vol. 43, pp.80–87.
- Qiu, R.C., Scholtz, R. and Shen, X. (2005b) 'Ultra-wideband wireless communications – a new horizon', *IEEE Trans. Veh. Technol., Editorial on Special Issue on UWB*, Vol. 54, September.
- Qiu, R.C., Zhou, C. and Liu, Q. (2005c) 'Physics-based pulse distortion for ultra-wideband signals', *IEEE Trans. Veh. Tech.*, September, Vol. 54, No. 5, pp.1546–1554.
- Qiu, R.C., Zhang, J.Q. and Guo, N. (2006a) 'Detection of physics-based ultra-wideband signals using generalized RAKE and multi-user detection (MUD)', *IEEE J. Selected Areas in Commun. (JSAC), the Second JSAC Special Issue on UWB Radio*, May, Vol. 24.
- Qiu, R.C., Zhou, C., Guo, N. and Zhang, J.Q. (2006b) 'Time reversal with MISO for ultra-wideband communications: experimental results (invited paper)', *IEEE Radio and Wireless Symposium*, San Diego, CA.
- Qiu, R.C., Zhou, C., Zhang, J.Q. and Guo, N. (2006c) 'Channel reciprocity and time-reversed propagation for ultra-wideband communications', *IEEE Antenna and Wireless Propagation Letters*, Vol. 5, No. 1, pp.269–273.
- Qiu, R.C. and et al. (2007a) *Ultra-wideband Communications Systems and Testbed*, Tech. Rep., Final Report to Army Research Office, Grant No. W911NF-05-01-0111, 240 pages, TTU, Cookeville, TN, July.
- Qiu, R.C., Sadler, B.M. and Hu, Z. (2007b) 'Time reversed transmission with chirp signalling for UWB communications and its application in confined metal environments', *International Conference on Ultra-wideband, ICUWB'07*, Singapore, September.
- Qiu, R.C., Zhou, C., Guo, N. and Zhang, J.Q. (2006) 'Time reversal with MISO for ultra-wideband communications: experimental results', *IEEE Antenna and Wireless Propagation Letters*, Vol. 5, pp.269–273.
- Qiu, R.C., Zhou, C., Zhang, J.Q. and Guo, N. (2007c) 'Channel reciprocity and time-reversed propagation for ultra-wideband communications', *IEEE AP-S International Symposium on Antennas and Propagation*, Honolulu, Hawaii, June, Vol. 1.
- Rousseau, P.R. and Pathak, P.H. (1996) *Time Domain Version of the Uniform Geometrical Theory of Diffraction*, The Ohio State University, Technical Report 721564-3, Tech. Rep., February.
- Rousseau, P.R. and Pathak, P.H. (1995) 'Time domain uniform geometrical theory of diffraction for a curved wedge,' *IEEE Trans. Antenna Prop.*, December, Vol. 43, No. 12, pp.1375–1382.
- Roy, S., Foerster, J., Somayazulu, V. and Leeper, D. (2004) 'Ultra-wideband radio design: the promise of high-speed, short range wireless connectivity', *Proceedings of the IEEE*, February, Vol. 92, pp.295–311.
- Scholtz, R. (1993) 'Multiple access with time-hopping impulse modulator (invited paper)', *MILCOM'93*, October, pp.11–14.
- Shen, X., Guizani, M., Chen, H., Qiu, R.C. and Molisch, A. (2006) 'Ultra-wideband wireless communications', *IEEE J. Select. Areas Commun., Editorial on Special Issue on UWB*, 2nd Quarter, Vol. 24.
- Slepian, D. and Pollak, H.O. (1961) 'Prolate spheroidal wave functions, Fourier analysis and uncertainty-1', *Bell Syst. Tech. J.*, January, Vol. 40, No. 1, pp.4346.
- Van Trees, H.L. (1968) *Detection, Estimation and Modulation Theory, Part I*, Wiley, New York.
- Veruttipong, T.W. (1990) 'Time domain version of the uniform GTD', *IEEE Trans. Antenna Prop.*, November, Vol. 38, No. 11, pp.1757–1764.
- Win, M. and Scholtz, R. (2000) 'Ultra-wide bandwidth time-hopping spread spectrum impulse radio for wireless multiple-access communications', *IEEE Trans. Commun.*, April, Vol. 48, pp.679–689.
- Zhang, H., Zhou, X., Yazdandoost, K.Y. and Chalamtac, I. (2006) 'Multiple signal waveforms adaptation in cognitive ultra-wideband radio evolution', *IEEE Journal on Selected Areas in Communications (JSAC)*, April, Vol. 24, No. 4.
- Zhou, C. and Qiu, R.C. (2006a) 'Spatial focusing of time-reversed UWB electromagnetic waves in a hallway environment', *In System Theory, 2006, Proceeding of the Thirty-Eighth Southeastern Symposium*, pp.318–322.
- Zhou, C. and Qiu, R.C. (2006b) 'Spatial focusing of time-reversed UWB electromagnetic waves in a hallway environment', *IEEE 38th Southeastern Symposium on System Theory*, Cookeville, TN, USA, 5–7 March.

- Zhou, C. and Qiu, R.C. (2007) 'Pulse distortion caused by cylinder diffraction and its impact on UWB communications', *IEEE Trans. Veh. Techn.*, July, Vol. 56, No. 4, pp.2385–2391.
- Zhou, C., Guo, N. and Qiu, R.C. (2007a) 'A study on time reversed impulse UWB with multiple antennas based on measured spatial UWB channels', *IEEE Trans. Vehicular Tech.*, submitted for publication.
- Zhou, C., Sadler, B.M. and Qiu, R.C. (2007b) 'Performance study on time reversed impulse MIMO for UWB communications based on realistic channels', *IEEE Conf. Military Comm., MILCOM'07*, October, Orlando, FL.